Electronic Supplementary Material (ESI) for Dalton Transactions.
This journal is © The Royal Society of Chemistry 2018

**Supporting information**

# $H_5PV_2Mo_{10}O_{40}$ Encapsulated in MIL-101(Cr): Facile Synthesis, Characterization of Rationally Designed Composite Materials for Efficient Decontamination of Sulfur Mustard under Ambient Conditions

Yanqin Li,[a†] Qi Gao,[a†] Lijuan Zhang,[*a] Yunshan Zhou,[*a] Yuxu Zhong,[*b] Ying Ying,[b] Mingcai Zhang,[a] Chunqian Huang,[b] and Yong'an Wang[b]

[a]State Key Laboratory of Chemical Resource Engineering, Institute of Science, Beijing University of Chemical Technology, Beijing 100029, P. R. China; [b]State Key Laboratory of Toxicology and Medical Counter measures, Institute of Pharmacology and Toxicology, Academy of Military Sciences PLA China, Beijing 100850, P. R. China

**Table S1**. Composition of the HD-containing standard solutions.

| Entry | Diluted HD solution (μL) | Petroleum ether (μL) | The blue reagent (μL) | Absolute ethyl alcohol (μL) |
|---|---|---|---|---|
| B1 | 0 | 100 | 200 | 100 |
| B2 | 20 | 80 | 200 | 100 |
| B3 | 40 | 60 | 200 | 100 |
| B4 | 60 | 40 | 200 | 100 |
| B5 | 80 | 20 | 200 | 100 |
| B6 | 100 | 0 | 200 | 100 |

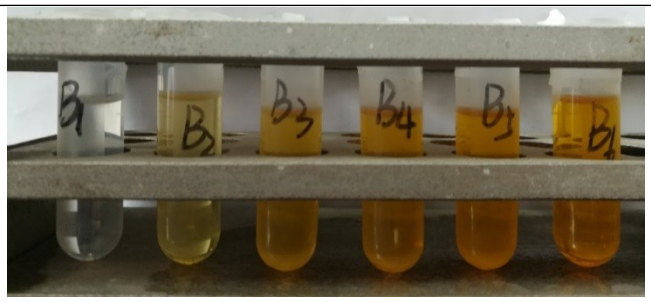


**Figure S1**. Photograph of the HD-containing standard solutions of different concentrations (B1 → B6).

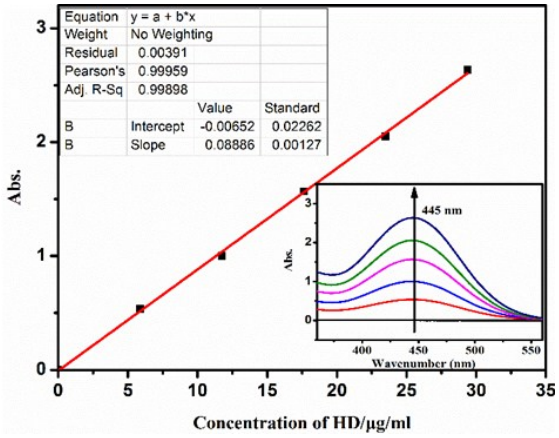


**Figure S2**. Calibration curve of UV-vis. absorbance of the HD-containing solution. Insert image is UV absorbance of HD-containing standard solution at 445 nm versus concentration of HD.

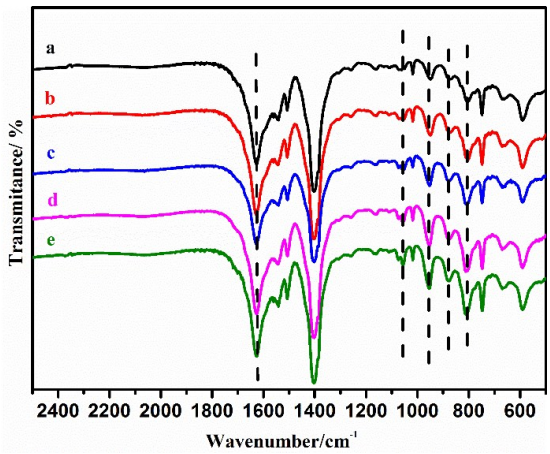


**Figure S3**. IR spectra of the composites $H_5PV_2Mo_{10}O_{40}$@MIL-101(Cr): **1a** (line a), **1b** (line b), **1c** (line c), **1d** (line d), **1e** (line e).

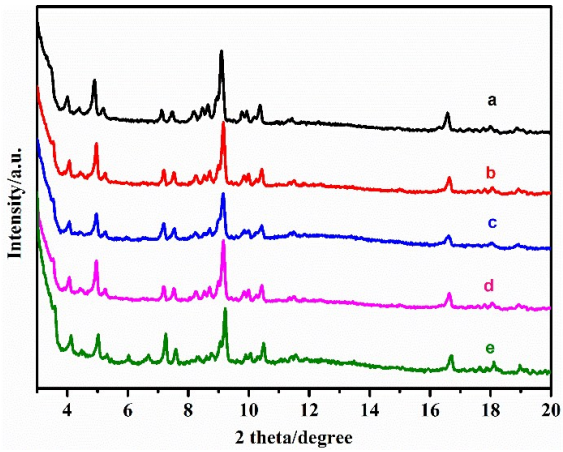


**Figure S4**. Powder XRD patterns of the composites $H_5PV_2Mo_{10}O_{40}$@MIL-101(Cr): **1a** (line a), **1b** (line b), **1c** (line c), **1d** (line d), **1e** (line e).

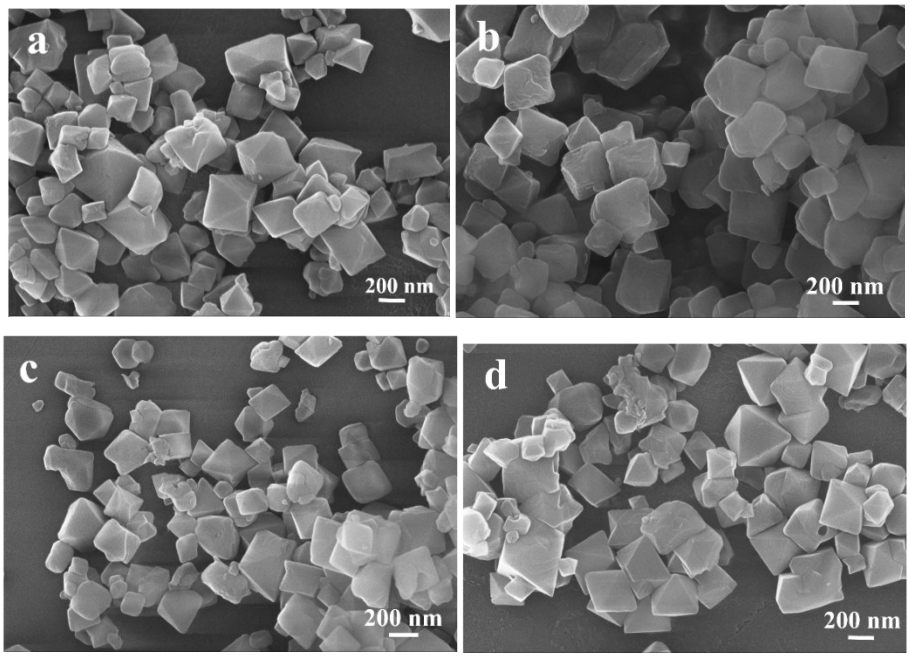


**Figure S5**. SEM images of the composites $H_5PV_2Mo_{10}O_{40}$@MIL-101(Cr): **1a** (a), **1b** (b), **1c** (c), and **1e** (d).

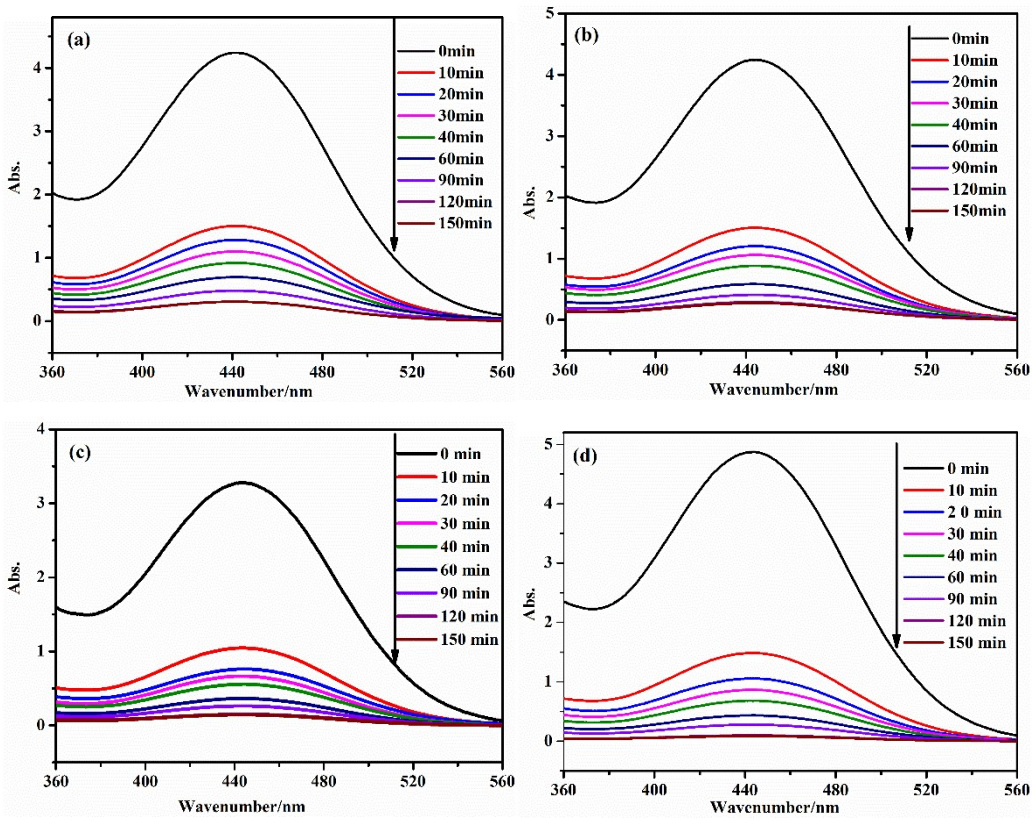


**Figure S6**. UV-vis. absorption curves of residual HD-containing solutions after decontamination on MIL-101(Cr) (a), the composites **1a** (b), **1b** (c), and **1c** (d) at different time.

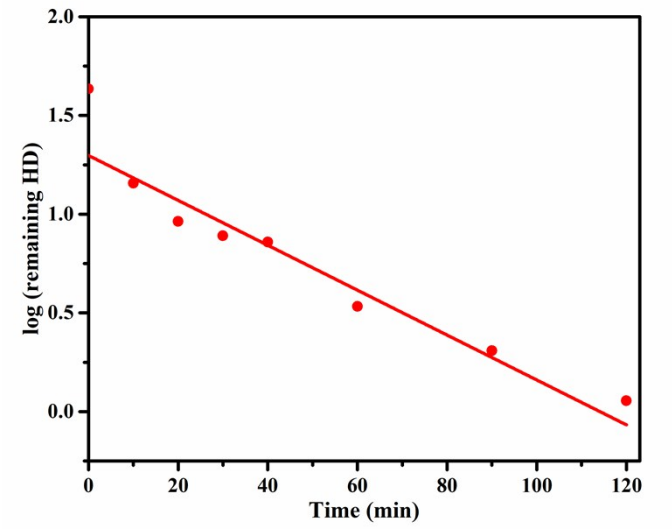


**Figure S7**. Kinetics of degradation of HD on composite 1d.

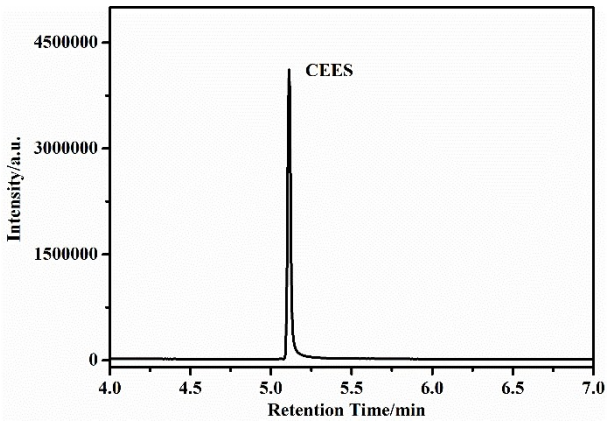


**Figure S8**. GC spectrum of the extracted suspension from 2-CEES decontaminated by MIL-101(Cr).

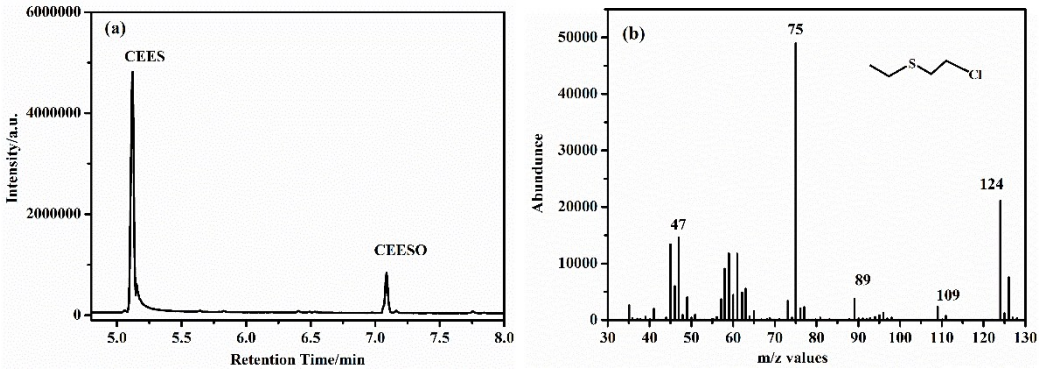


**Figure S9**. The GC–MS spectra of the products extracted from the 2-CEES solution after being decontaminated by the composite **1d**: GC spectrum (a), mass spectrum for CEES (b).

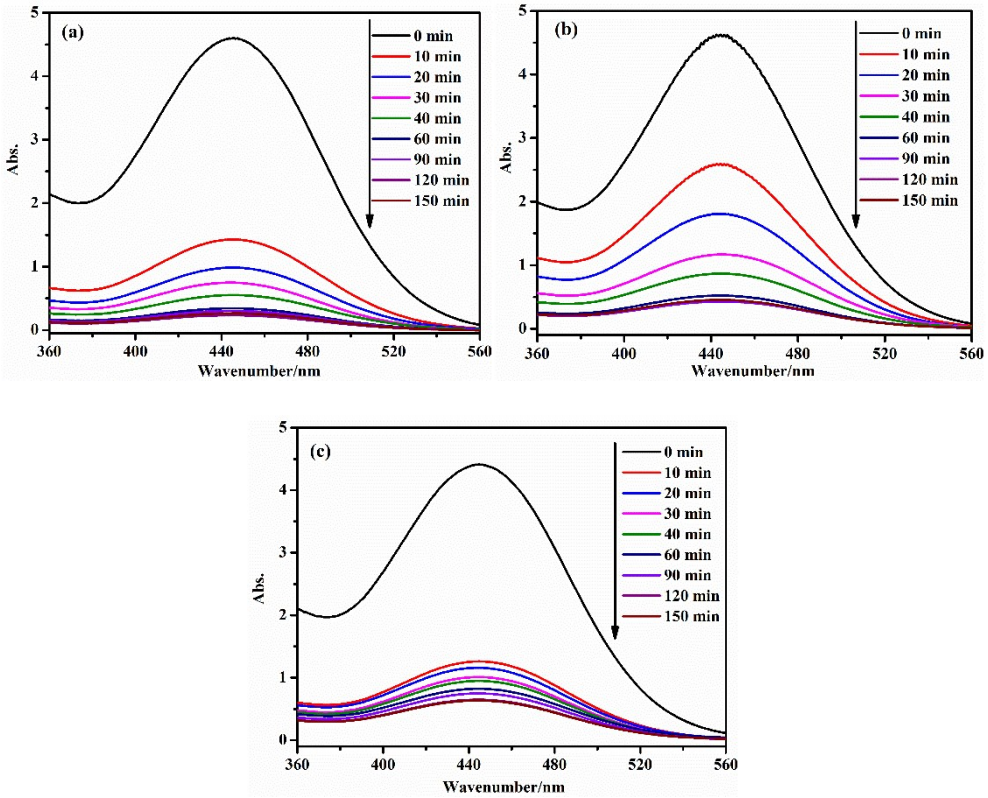


**Figure S10**. UV-vis absorption curves of residual HD-containing solutions after decontamination on nano-$Al_2O_3$ (a), nano-Mg (b), and activated clay (c).

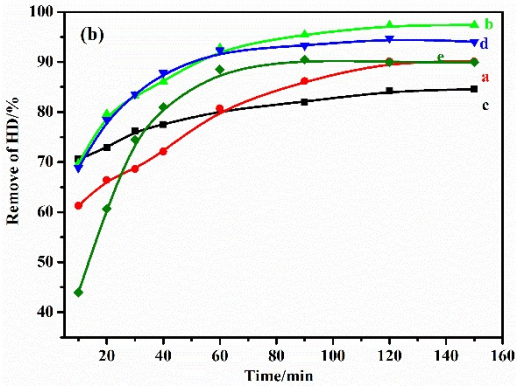


**Figure S11.** The decontamination efficiency of HD on MIL-101(Cr) (red line a), the composite **1d** (bright green line b), activated clay (black line c), nano-$Al_2O_3$ (blue line d) and nano-MgO (dark green line e), respectively. The experimental conditions: 25 ℃, amount: 20mg, HD initial concentration 0.116g/ml, 44 μl.

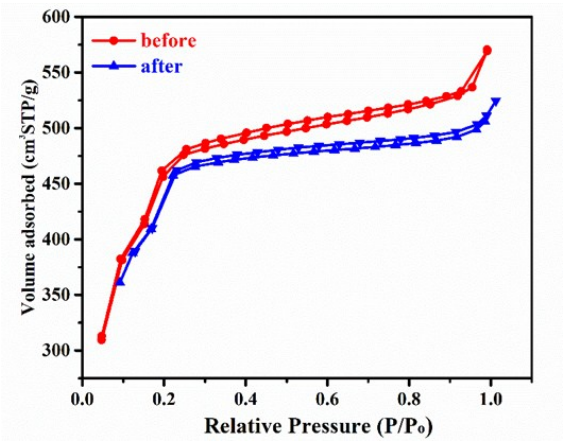


**Figure S12**. N2 adsorption isotherms of the of the freshly prepared composite **1d** and fourth regenerated composite **1d**.

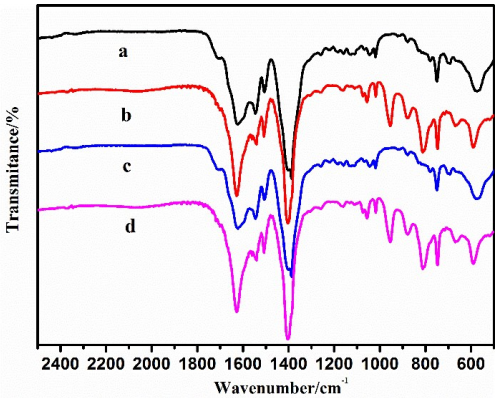


**Figure S13**. IR spectra of the freshly prepared MIL-101(Cr) (line a), the composite **1d** (line b), fourth regenerated MIL-101(Cr) (line c) and the composite **1d** (line d).

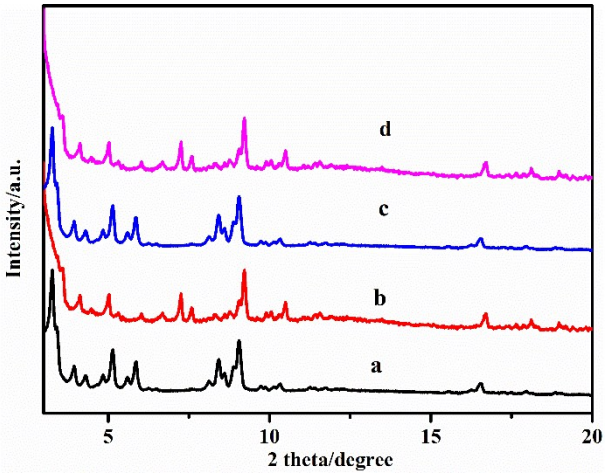


**Figure S14**. Powder XRD spectra of the freshly prepared MIL-101(Cr) (line a) and the composite **1d** (line b) and fourth regenerated MIL-101(Cr) (line c) and the composite **1d** (line d).

**Scheme S1.** Schematic representation of mass fragmentation pattern of CEES

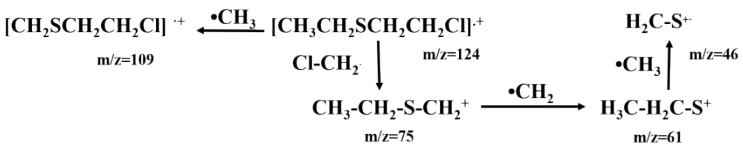

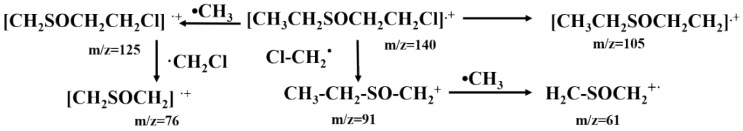
**Scheme S2.**Schematic representation of mass fragmentation pattern of CEESO